



# Multiscale MHD simulation of a coronal mass ejection and its interaction with the magnetosphere–ionosphere system

T.I. Gombosi<sup>a,\*</sup>, D.L. DeZeeuw<sup>a</sup>, C.P.T. Groth<sup>a,1</sup>, K.G. Powell<sup>b</sup>, Q.F. Stout<sup>c</sup>

<sup>a</sup>*Department of Atmospheric, Oceanic and Space Sciences, The University of Michigan, Ann Arbor, MI 48109, USA*

<sup>b</sup>*Department of Aerospace Engineering, The University of Michigan, Ann Arbor, MI 48109, USA*

<sup>c</sup>*Department of Electrical Engineering and Computer Science, The University of Michigan, Ann Arbor, MI 48109, USA*

Received 15 January 2000; accepted 15 March 2000

## Abstract

We report on the first comprehensive numerical simulation of a space weather event, starting with the generation of a CME and subsequently following this transient solar wind disturbance as it evolves into a magnetic cloud and travels through interplanetary space towards Earth where its interaction with the terrestrial magnetosphere–ionosphere system is also predicted as part of the simulation. © 2000 Elsevier Science Ltd. All rights reserved.

*Keywords:* MHD; Coronal mass ejection; Magnetic cloud; Magnetosphere–Ionosphere

## 1. Introduction

Global computational models based on first principles represent a very important component of efforts to understand the intricate processes coupling the Sun to the geospace environment. The hope for such models is that they will eventually fill the gaps left by measurements, extending the spatially and temporarily limited observational database into a self-consistent global understanding of our space environment.

Presently, and in the foreseeable future, magnetohydrodynamic (MHD) models are the only models that can span the enormous distances present in the magnetosphere. However, it should not be forgotten that even generalized MHD equations are only a relatively low-order approximation to more complete physics; they provide only a simplified description of natural phenomena in space plasmas.

MHD codes have been used successfully to model many important processes in the solar corona, the interplanetary medium and the Earth's magnetosphere. In spite of its inherent limitations, MHD represents a powerful global modeling tool which has significantly advanced our understanding of the geospace environment. During the last decade impressive progress was achieved in global 3D MHD models describing the solar corona (cf. Usmanov, 1995; Linker and Mikić, 1995; Linker et al., 1999), the inner heliosphere (cf. Pizzo, 1991; Odstrčil and Pizzo, 1999b,c), and the magnetosphere–ionosphere system (cf. Ogino and Walker, 1984; Lyon et al., 1986; Raeder et al., 1995; Tanaka, 1995; Janhunen, 1996; Gombosi et al., 1998; White et al., 1998). However, no attempt has been made so far to simulate the entire region extending from the lower solar corona through the heliosphere to the magnetosphere–ionosphere system in a single calculation.

In this paper, we describe the first comprehensive numerical simulation of the Sun–earth system, starting with the generation of a CME in a background solar wind, and subsequently following this transient solar wind disturbance as it evolves into a magnetic cloud and travels through interplanetary space towards Earth where its interaction with the terrestrial magnetosphere is also predicted as part of the simulation.

\* Corresponding author. Tel.: 1-734-764-7222; fax: 1-734-647-3083.

*E-mail address:* [tamas@umich.edu](mailto:tamas@umich.edu) (T.I. Gombosi).

<sup>1</sup> Presently at Institute of Aerospace Studies, University of Toronto.

## 2. Simulation code

The BATS-R-US code solves the governing equations of magnetohydrodynamics. Terms describing deviations from ideal MHD are included through appropriate source terms. The BATS-R-US code has the capability to include the effects of solar rotation, solar gravity, a multipole intrinsic solar magnetic field (up to octupole), as well as including user-defined volumetric heating or energy sources. Detailed description of the code and its validation can be found in Powell et al. (1999) and Groth et al. (1999). The high-resolution finite volume solution scheme is based on an approximate Riemann solver for magnetohydrodynamics (Powell, 1994; Powell et al., 1995). In this approach, the hydrodynamic and electromagnetic effects are solved for in a fully three-dimensional (no dimensional splitting) tightly coupled manner, rather than in separate steps (Gombosi et al., 1994; Powell et al., 1995, 1999; Groth et al., 1999). The resulting scheme works equally well across a range of several orders of magnitude in plasma  $\beta$ .

The basic data structure used in the BATS-R-US approach is that of adaptive blocks. Adaptive blocks partition space into regions, each of which is a regular Cartesian grid of cells, called a block. If the region needs to be refined, then the block is replaced by 8 child subblocks (one for each octant of the parent block), each of which is a Cartesian grid of cells containing the same number of cells as the parent block. If coarsening is needed, then the 8 children are replaced by their parent. The blocks in the grid, at their various levels of refinement, are stored in a tree-like data structure.

For solar wind–magnetosphere interaction modeling, it is important to take the coupling between the magnetosphere and ionosphere into account. This is done herein through an electrostatic ionosphere model in which it is assumed that magnetospheric field-aligned currents can penetrate into a height-integrated electrostatic ionosphere. Current closure is calculated using Ohm's law with a height-integrated conductivity (conductance) tensor (Goodman, 1995; Amm, 1996). Once the ionospheric electrostatic potential is derived, one can calculate the ionospheric convection velocity, which is used as boundary condition for the magnetosphere simulation at the magnetosphere–ionosphere interface (in addition to the velocity due to planetary rotation).

## 3. Simulation domain

The computational domain used in the calculation is a heliocentric rectangular box defined by  $-32R_{\odot} \leq x \leq 224R_{\odot}$ ,  $-192R_{\odot} \leq y \leq 192R_{\odot}$ ,  $-192R_{\odot} \leq z \leq 192R_{\odot}$ . The adapted computational grid for the initial solution of the solar wind (which is a steady-state solution in the corotating frame) consists of 15,768 self-similar  $4 \times 4 \times 4$  blocks and 1,009,152 cells with 8 refinement levels and a minimum cell size at the solar surface of  $1/16R_{\odot}$ . During

the time-dependent calculation of the CME, the grid dynamically adapted to the varying solution according to the refinement criteria and the size of the computational mesh varied from under 800,000 cells to in excess of 2,000,000 cells. The length of the entire simulation was 120 h starting from the initiation of the CME ( $t = 0$ ).

The procedure for prescribing boundary conditions at the solar surface is dependent on local flow conditions. Plasma can freely leave the reservoir, but no “backflow” is allowed. In addition, no deviation is allowed from the intrinsic magnetic field at the interface. At the outer boundaries of the rectangular solution domain, the solar wind flow is essentially super-fast (and hence super-Alfvénic). Simple zero-gradient or constant extrapolation boundary conditions are therefore appropriate and are used to specify the plasma properties at the outer boundary. A detailed description of the boundary conditions can be found in Groth et al. (2000).

The resolution of the initial computational grid at Earth is approximately  $10R_{\oplus}$ , but during the passage of the interplanetary transient this resolution increased by about a factor of four. The embedded magnetosphere is simulated in a moving computational box defined by  $-384R_E \leq x \leq 128R_E$ ,  $-128R_E \leq y \leq 128R_E$ ,  $-128R_E \leq z \leq 128R_E$  with 8 levels of refinement, 2004 self-similar blocks of  $4 \times 4 \times 4$  cells and 128,256 computational cells. The magnetosphere is “turned on” for a total of 27 h starting at  $t = 70$  h.

The inner boundary of the magnetosphere simulation is a sphere at  $3R_E$ . This sphere is connected to the height-integrated electrostatic ionosphere as described earlier in this paper.

## 4. The inner heliosphere near solar minimum

An initial solution representative of the state of the solar wind before the initiation of the CME is required as a starting point for this simulation of a space weather event. A “pre-event” solution has been developed for these purposes using the BATS-R-US simulation code which attempts to reproduce many of the observed global features of solar corona and the inner heliosphere for conditions near solar minimum.

Observations have shown that the solar wind is fundamentally a two-state phenomenon (cf. Axford and McKenzie, 1997, and references therein). The so-called high-speed or *fast solar wind* is usually observed in the high-latitude regions of the heliosphere, while the so-called *slow solar wind* is confined to relatively low latitudes. There is general agreement that the fast solar wind originates from polar coronal holes and it is thought to be generated by additional heating above the transition region but close to the Sun (cf. Axford and McKenzie, 1996; Fisk et al., 1999b).

The slow solar wind is confined to a narrow region near the heliospheric current sheet (McComas et al., 1998; Neugebauer et al., 1998). This highly variable slow wind is thought to be formed from material stored in closed

magnetic field structures and subsequently opened due to magnetic reconnection (cf. Fisk et al., 1999a; Schwadron et al., 1999). The fast-latitude scan of Ulysses showed very sharp transitions between the fast and slow solar winds (cf. McComas et al., 1998).

In the first part of our simulation we attempted to reproduce the three-dimensional bulk features of the solar wind for solar minimum conditions. We applied the BATS-R-US simulation code to solve the three-dimensional ideal MHD equations from the solar surface to beyond Earth's orbit. BATS-R-US has the capability to include the effects of solar rotation, solar gravity, a multipole intrinsic magnetic field (up to octupole), as well as including user-defined volumetric sources of mass, momentum and energy. This feature is very important in the present simulation, since BATS-R-US solves the full MHD energy equation and uses  $\gamma = \frac{5}{3}$  for the ratio of specific heats (since ideal MHD assumes perfect gases).

For the purposes of the present simulation, it is assumed that at the top of transition region, at a radial distance of  $1R_{\odot}$ , the base of the solar corona is a large rigidly rotating reservoir of hot, stationary plasma with an embedded magnetic multipole field. The plasma temperature (the sum of the ion and electron temperatures) in the reservoir is taken to be  $T_{\odot} = 2.85 \times 10^6$  K and the plasma density is assumed to be  $n_{\odot} = 1.5 \times 10^8 \text{ cm}^{-3}$ .

The intrinsic solar magnetic field at the solar surface is defined in terms of a multipole expansion that includes terms up to the octupole moment. In the present simulation there was no quadrupole moment, while the octupole and dipole were tilted in the  $(x, z)$  plane of the corotating coordinate system. The magnetic axis tilt angle was  $-15^{\circ}$  and the solar magnetic field was azimuthally symmetric about the magnetic axis. The surface field strength was 8.4 G at the magnetic poles and 2 G at the solar magnetic equator.

Some of our early numerical experiments with the solar wind made it clear that additional energy input in the form of a volumetric heat source is needed beyond the solar surface to simulate a realistic solar wind in three dimensions. In our initial attempts to model the expansion of plasma from the solar reservoir without volumetric source of energy and momentum, we obtained hydrostatic-type solutions as long as the plasma temperature ( $T_{\odot} = T_e + T_p$ ) in the reservoir was less than about 10–12 million K. Once the reservoir temperature was increased above this critical value we obtained plasma outflow from the entire solar surface. This result is consistent with Parker's original predictions (Parker, 1963). Without additional heat input the plasma parameters at 1 AU were very different from the parameter regime we expect from the solar wind: the speed was over 2000 km/s, and the density and magnetic field magnitude were orders of magnitude off. Even though there is general agreement about the need of such a heat input (cf. Axford and McKenzie, 1996; Fisk et al., 1999b), the nature of such energy input is still debated (cf. Holzer et al., 1997). An additional difficulty with finding the appropriate parametric volume heat

source function is the fact the ideal MHD neglects the effects of heat conduction. In reality, this is a very important effect near the Sun, where the solar wind is accelerated (cf. Hu et al., 1997; Steinolfson, 1994; Suess et al., 1996; Moore et al., 1999).

In our simulations, the role of the volumetric heating function is to mimic the combined effects of energy absorption above the transition region, heat conduction (which is not included in ideal MHD) and radiative losses. Presently, the physical understanding of these processes is quite limited, therefore one has considerable freedom in choosing the volumetric heating function. Our approach is to reverse the problem and see whether one can find a heating function which results in reasonable plasma parameters near the Sun and around 1 AU. We adopted a heating function that includes both local energy depositions and losses, thus mimicking the real situation in the lower corona. Specifically, the heating function was assumed to be proportional to  $(T_0 - T)$ , where  $T_0$  is a prespecified "target" temperature. We have chosen  $T_0 = 1.75T_{\odot}$  inside the coronal hole and  $T_0 = T_{\odot}$  outside (the coronal hole boundary was at  $72.5^{\circ}$  latitude). We note that our heating function has a sharp gradient at the edge of the coronal hole, however, the resolution of the computational grid (about  $5^{\circ}$  near the Sun) limits the sharpness of the transition. Finally, the heating scale-height slowly varies from about  $4.5R_{\odot}$  near the equator to about  $9R_{\odot}$  at the poles. Overall, the motivation for this choice of heating function was to reproduce many of the observed global plasma properties of the solar wind. A detailed description of the heating function is given in Groth et al. (2000).

As it was mentioned earlier, the slow solar wind is thought to be an inherently transient phenomenon that is continuously formed from closed magnetic structures which are opened through reconnection (Fisk, 1996; Schwadron et al., 1999). It is quite difficult to simulate this effect in ideal MHD. However, discretization of the equations (which is necessary for numerical solution) introduces numerical dissipation into the solution. BATS-R-US uses a solution method which minimizes numerical dissipation, but requires finite resistivity for numerical stability. This small amount of numerical resistivity results in reconnection of magnetic field lines at the top of the helmet-like last closed magnetic field lines (this reconnection continues along the heliospheric current sheet). This reconnection results in the generation of a slow solar wind near the magnetic equator. In some respect, the numerical resistivity is helpful in "mimicking" some of the real physical process taking place near the Sun.

Fig. 1 shows a 3D representation of the initial solution for the pre-event solar wind near the Sun. The solution is shown in the meridional and equatorial cuts (the  $(x, z)$  and  $(x, y)$  planes, where the  $z$ -axis is along the rotation axis, while the magnetic axis is in the  $(x, z)$  plane). The color code represents the logarithm of the magnitude of the magnetic field (in units of G) in the two planes. Solid lines are magnetic field lines: magenta denotes the last closed field lines, red

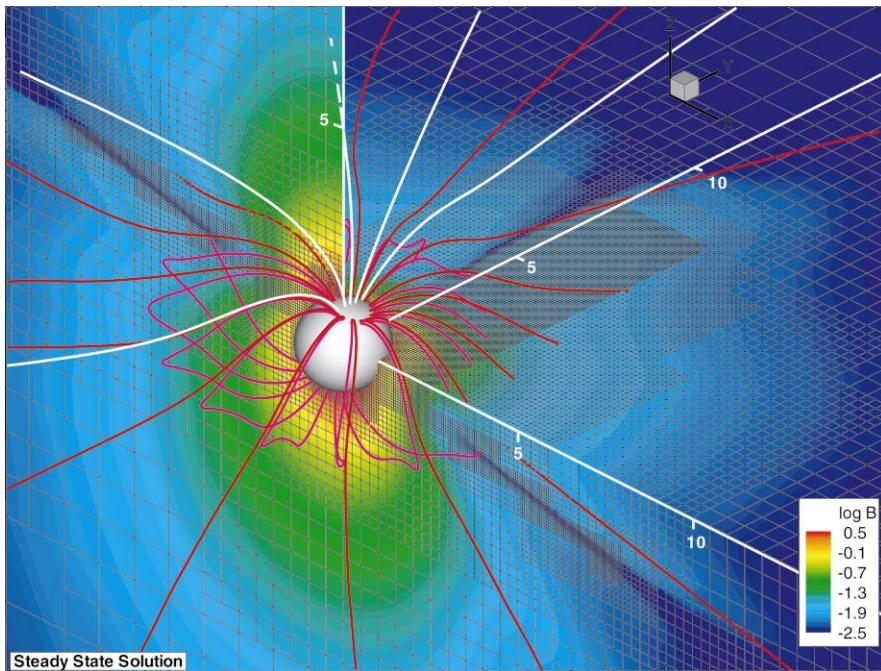


Fig. 1. 3D representation of the near-solar region before the initiation of the CME. The color code represents  $\log(B)$  in the  $(x,z)$  and  $(x,y)$  planes. Solid lines are magnetic field lines: magenta denotes the last closed field lines, red is open field lines expanding to the interplanetary medium just above the heliospheric current sheet, and finally, white lines show open magnetic field lines in the  $(y,z)$  plane.

is open field lines expanding to the interplanetary medium just above the heliospheric current sheet, and finally, white lines show open magnetic field lines in the  $(y,z)$  plane.

The narrow dark blue region in Fig. 1 is the beginning of the heliospheric current sheet. It originates around  $4R_{\odot}$  where the equatorial portion of the closed magnetic field lines become highly stretched, and extends throughout the entire solution. The current sheet is warped and tilted due to the combined effect of magnetic tilt and rigid solar rotation.

The solution, which is dictated by the complex balance of pressure, magnetic, gravitational, and inertial forces, has regions of open and closed magnetic field lines and leads to the formation of a “helmet” streamer magnetic streamer configuration with associated neutral point and equatorial current sheet. The solution correctly mimics some of the dual state features of the solar wind. It produces fast solar wind ( $\sim 800$  km/s) above  $\sim 30^{\circ}$  heliolatitude, slow ( $\sim 400$  km/s) solar wind near the solar equator, and provides reasonable values for the solar wind temperature and density and interplanetary magnetic field at 1 AU.

As evidence of this two-state nature of the solution, we present Fig. 2. Fig. 2 shows the observed and simulated meridional cross sections of the solar wind speed. The observations come from the Ulysses spacecraft (McComas et al., 1998). The thick lines are a polar diagram of the asymptotic values of the computed solar wind speed as a function of heliolatitude. As a consequence of the magnetic

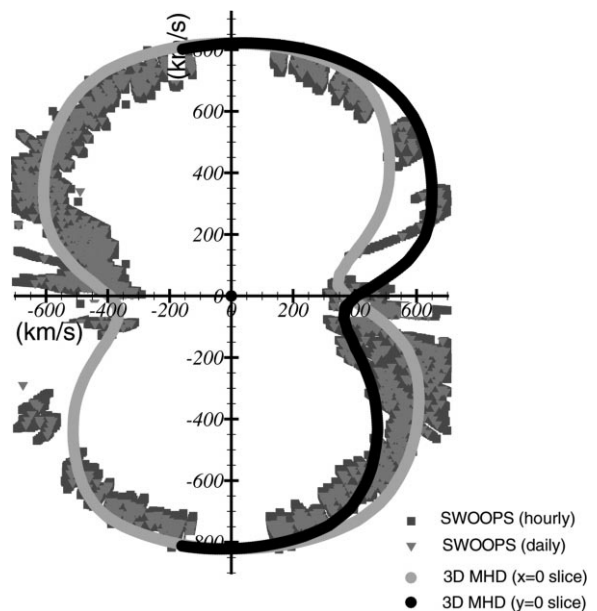


Fig. 2. Predicted solar wind velocity and stream lines and polar plot of the asymptotic value of the computed solar wind speed compared to the observations of the Ulysses/SWOOPS instrument (McComas et al., 1998).

tilt and solar rotation the simulated meridional speed profile is different in different meridional cuts. In Fig. 2 we show two speed profiles in the  $x=0$  (green) and  $y=0$  (black) planes. It is interesting to note that at high latitudes (in the fast solar wind region) the two meridional profiles show practically identical speeds, while at lower latitudes the meridional profiles differ by as much as 200 km/s. As the Sun rotates a slow moving observer located at mid-latitudes (such as the Ulysses spacecraft) detects a rapid transition from one solar wind regime to another. The observed transition time is basically controlled by the thickness of the heliospheric current sheet. We note that the simulation is quite consistent with Ulysses observations (McComas et al., 1998).

Overall, our initial condition represents a very reasonable description of three-dimensional inner heliosphere for solar minimum conditions. We used physically reasonable input parameters near the Sun and were able to obtain a solution out to 1 AU which is in good overall agreement with average observed solar wind conditions.

## 5. Simulation of a CME

Coronal mass ejections (CMEs) are highly transient solar events involving the expulsion of mass and magnetic field from the solar surface. On the order of  $10^{12}$  kg of plasma may be expelled from the solar surface during a typical event. These dynamic events originate in closed magnetic field regions of the corona. They produce large-scale reconfiguration of the coronal magnetic field and generate large solar wind disturbances that, as mentioned above, appear to be the primary cause of major geomagnetic storms at Earth.

The physical mechanisms involved in the initiation of CMEs are not well understood. Many scenarios have been put forth for their release. Early on it was suggested that thermally driven pressure pulses from solar flares drive the release (e.g. Dryer et al., 1979), yet more recently it is felt that it is the large-scale destabilization of the coronal magnetic field that initiates CMEs. Low (1990) and Hundhausen (1995) have recently considered the release of CMEs as a two-step process: first, there is a CME which opens up an initially closed coronal magnetic field; this is followed by a flare resulting from the reconnective-closing of field lines trailing the ejecta (Hirayama, 1974; Kopp and Pneuman, 1976; Low, 1994). Another scenario put forth for the formation and release of CMEs involves the buildup of magnetic energy and subsequent destabilization of the field due to the quasi-static shearing of the footprints of closed magnetic field lines on the solar surface (Low, 1977; Wu et al., 1983; Mikić et al., 1988; Mikić and Linker, 1994). This effect is likely to be a trigger mechanism but is not, by itself, sufficient to explain the CME phenomenon (Linker and Mikić, 1995; Low, 1996). Finally, it has been suggested that the onset of CMEs may be produced by the emergence of magnetic flux ropes that gain energy as they are continually stressed and deformed by chromospheric and photospheric motions

(van Ballegooijen and Martens, 1990). Prior to eruption, the flux ropes are confined by the large mass in the flux tubes, but when confinement fails CMEs are initiated due to the magnetic buoyancy of the ropes (Low, 1981; Fisher and Poland, 1981; Low et al., 1982; Illing and Hundhausen, 1986).

After release, CMEs accelerate and become part of the outward flow of the solar wind. They are either accelerated by the solar wind so as to come into equilibrium with the ambient wind or act as drivers moving faster than the background solar wind. Close to the Sun, the typical dimension of a CME is less than a solar radius. As the CMEs propagate outward from the corona, they expand dramatically and may extend over tenths of an AU by the time Earth's orbit is reached at 1 AU. Moreover, many, if not all, CMEs are associated with magnetic clouds and the plasma properties within these clouds can differ substantially from those of the ambient solar wind.

Global computational models based on first principles mathematical descriptions of the physics represent a very important component of efforts to understand the initiation, structure, and evolution of CMEs. Recent examples of the application of MHD models to the study of coronal and solar wind plasma flows include the studies by Steinolfson (1992,1994), Linker et al. (1994), Mikić and Linker (1994), Linker and Mikić (1995), Suess et al. (1996), Wang et al. (1998), Wu and Guo (1997), Guo and Wu (1998), Lionello et al. (1998), Dryer (1998), and Odstrčil and Pizzo (1999a,c).

Here we show our numerical results for a CME driven by local plasma density enhancement. This initial condition represents a simplified model of the situation just before eruption, when significant amount of mass is elevated into the lower corona. Later, we will apply more sophisticated initial conditions. At this time we just wanted to initiate a mass ejection and see how it moves through interplanetary space. In this calculation, the background solar wind solution described above was used as an initial solution and then a localized isothermal density enhancement was introduced at the solar surface just above the equatorial plane (as a consequence of the isothermal assumption the plasma pressure was also increased by the same factor as the density). This localized isothermal density enhancement initiated the CME. In this enhancement the density and pressure are locally increased by a factor of 135 in a small region just above the solar equator for a duration of about 12 h.

Fig. 3 shows a three-dimensional representation of the magnetic field configuration 9 h after the initiation of the CME. The color code represents  $\log(B)$ , white lines are open magnetic field lines, magenta lines represent magnetic field lines with both ends connected to the Sun. At this time the density enhancement is in the declining phase, but it is still more than 100 times higher than the background density. The density enhancement first leads to the "filling" of the closed magnetic field lines with additional plasma and subsequent expansion of the closed field line region. One can see that the closed field lines became greatly stretched by the outward

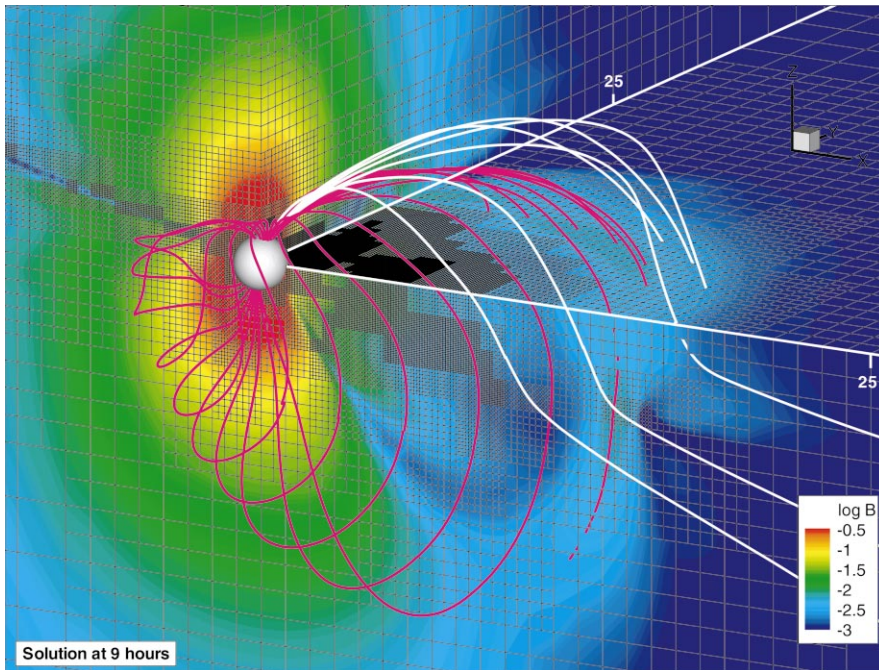


Fig. 3. 3D representation magnetic field lines 9 h after the initiation of a CME. Color code represents  $\log(B)$ , white lines are open magnetic field lines, magenta lines represent magnetic field lines with both ends connected to the Sun.

moving plasma. This is due to the fact that the plasma  $\beta$  (the ratio of the kinetic and magnetic pressures) is quite large and the magnetic field is “carried” by the outward moving plasma. We also note the decrease of magnetic field strength behind the leading edge of the outward moving disturbance.

A very interesting aspect of simulation results is the anisotropic expansion of the CME. The CME is fairly concentrated near the disrupted heliospheric current sheets, while it is broadly spread in the equatorial plane.

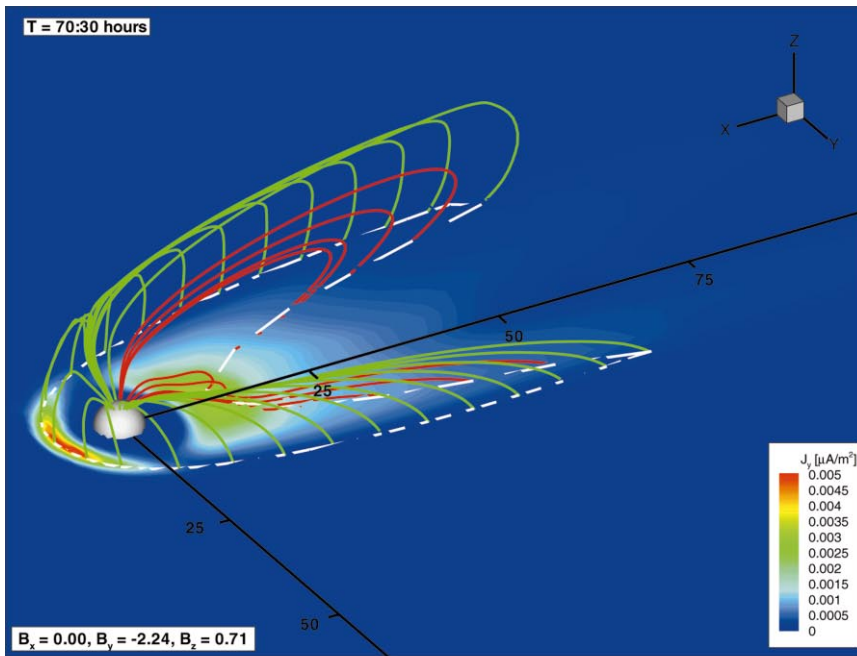
### 5.1. Interaction with the magnetosphere

The magnetosphere is a complex nonlinear system. The direction of the interplanetary magnetic field (IMF) fundamentally controls the large-scale topology of the magnetospheric configuration. The magnetospheric topology in turn controls the entry of mass, momentum, energy, and magnetic flux into the magnetosphere. The entry of these physical quantities from the solar wind into the magnetosphere produces various transition layers, the extended geomagnetic tail and the plasma sheet, current systems and auroral phenomena.

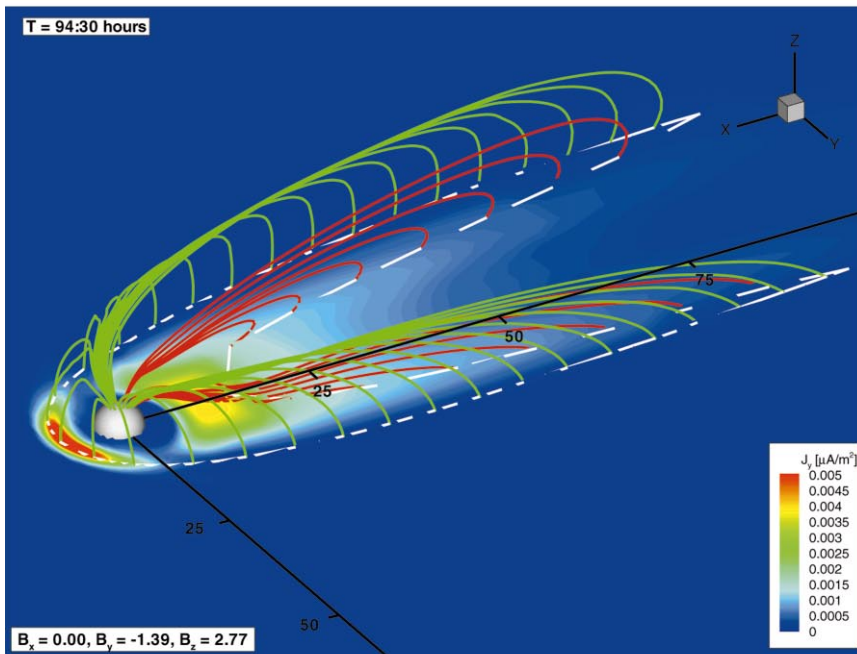
Three-dimensional global MHD simulations have been used for a long time to simulate the global magnetospheric configuration and to investigate the response of the magnetosphere–ionosphere system to changing solar wind conditions. The first global-scale 3D MHD simulations of the solar wind–magnetosphere system were published in the

early 1980s (LeBoeuf et al., 1981; Wu et al., 1981; Brecht et al., 1981,1982). Since then, global 3D MHD simulations have been used to study a range of processes, including the global magnetic field configuration, reconnection in the tail and at the dayside magnetopause, the dependence of magnetospheric convection on the orientation of the interplanetary magnetic field (IMF), and the self-excitation of auroral arcs (Ogino and Walker, 1984; Lyon et al., 1986; Ogino, 1986; Ogino et al., 1986; Fedder and Lyon, 1987; Ogino et al., 1989; Watanabe and Sato, 1990; Kageyama et al., 1992; Usadi et al., 1993; Walker et al., 1993; Fedder et al., 1995a,b; Berchem et al., 1995; Pulkkinen et al., 1995; Raeder et al., 1995; Tanaka, 1995; Janhunen and Koskinen, 1997; Raeder et al., 1997; Winglee et al., 1997; Gombosi et al., 1998,2000; Pulkkinen et al., 1998; White et al., 1998). A recent focus of recent global MHD investigations is the study of individual magnetospheric “events”. These simulations use observed upstream solar wind conditions to “drive” the magnetosphere–ionosphere system and compare the results with ground based or satellite observations (e.g., Fedder et al., 1995b,1998; Raeder et al., 1998).

Here, for the first time, we simulate the dynamic response of the global magnetospheric configuration to changing solar wind conditions self-consistently simulated all the way from the Sun to 1 AU. The solar wind changes at the location of the Earth due to the rotation of the tilted solar magnetic field and due to the passage of the coronal ejection described in the previous section.



(a)



(b)

Fig. 4. The response of the magnetosphere to the CME.

In the simulation Earth is assumed to move on a perfectly circular orbit about the Sun with an orbital radius of  $215.5R_s$  and an orbital period of 365.25 days. The orbital plane is assumed to be inclined at an angle of  $7.25^\circ$  to the solar equa-

tor with a node line aligned with the  $x$ -axis and the maximum and minimum excursions of the planet in  $z$ -direction occurring in the  $y = 0$  plane. Earth's initial position at  $t = 0$  in the numerical simulation is heliolatitude  $7.24^\circ$  and

longitude  $11.9^\circ$  (the CME takes place at  $0^\circ$  longitude and  $11.5^\circ$  latitude).

At this position Earth is located near the heliospheric current sheet when the CME is initiated. At Earth's location the first signatures of the CME can be seen in the magnetic field components at around 55 h after initiation. The driving mass (the piston) arrives around 72 h after the beginning of the event. The  $B_y$  component of the magnetic field remains pretty steady during the entire event, its value only changes by  $\sim 0.5$  nT. The  $B_x$  and  $B_z$  components, however, exhibit a significant rotation around the  $y$ -axis. This, in effect, is the signature of the passage of a CME-related flux rope. During the event the magnitude of the IMF increases from about 2 nT to approximately 4 nT. A more detailed description of the solar wind parameters at 1 AU is given in Groth et al. (2000).

The plasma temperature ( $T_e + T_p$ ) in the background solar wind is about  $2 \times 10^5$  K. During the CME (beginning at around 55 h) the plasma temperature significantly decreases dipping below  $1.5 \times 10^5$  K. The solar wind velocity remains nearly radial during the entire event with the speed gradually decreasing from about 550 to about 450 km/s. The undisturbed solar wind density is fairly high before the CME event ( $\sim 38 \text{ cm}^{-3}$ ), but it decreases to a more typical value of  $\sim 18 \text{ cm}^{-3}$  just at the arrival of the piston. At the peak of the event the density increases to about  $45 \text{ cm}^{-3}$ . The solar wind dynamic pressure increases from its pre-CME value of 2.25 nP (at 72 h) to 4.6 nP at the peak of the event.

Fig. 4 shows the change of the global magnetospheric configuration during the passage of the CME event. The figure shows two 3D snapshots at  $t = 70.5$  and  $94.5$  h. The color code represents the electric current density in the plane of the terrestrial equator, solid lines show last closed magnetic field lines. One can see the magnetopause current (or Chapman–Ferraro current) near the subsolar magnetopause and the tail current on the nightside.

The global magnetospheric configuration is primarily controlled by the  $B_z$  component of the interplanetary magnetic field. For  $B_z < 0$  the magnetosphere exhibits an open configuration with significant dayside reconnection and open magnetic field lines connected to large regions near the magnetic poles. For strong northward IMF conditions ( $B_z > 5$  nT) the magnetosphere becomes practically closed with magnetic reconnection limited to small regions near the cusps. For “intermediate” values of  $B_z$  (between about 0 and 5 nT) the global magnetospheric configuration is “partially closed” (or “partially open”). This configuration is characterized by significant dayside reconnection and large open cusps, by a narrow near-Earth reconnection line around the center of the magnetotail (the length of this reconnection line decreases with increasing  $B_z$ ), and by long, stretched magnetospheric wings connected to the dawn and dusk sides of the ionosphere. These magnetic wings are formed by highly stretched closed magnetic field lines. They represent the transition from magnetopause reconnection to tail reconnection. In Fig. 4 the last closed field lines at the

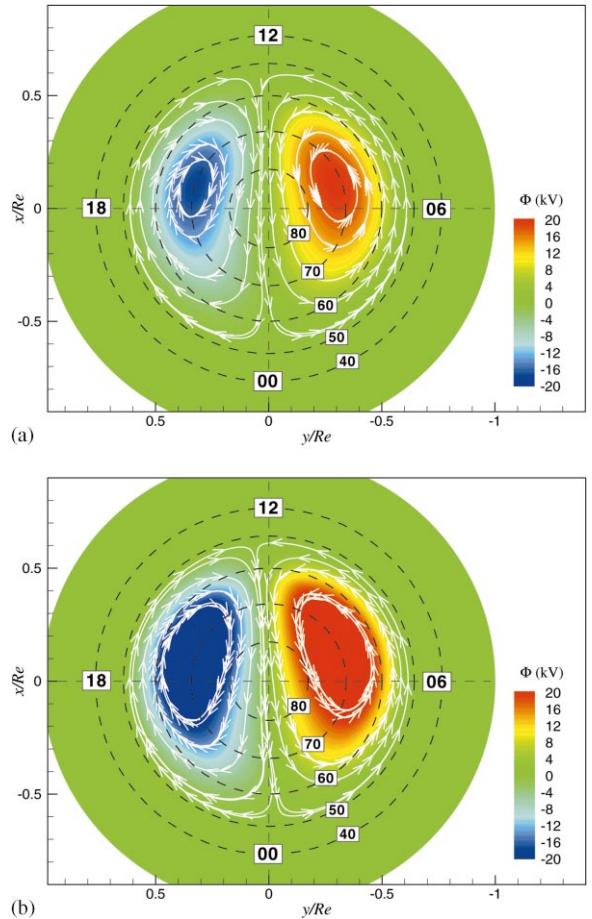


Fig. 5. Polar plot of the ionospheric convection (white lines) and potential distribution (color code) in the northern polar ionosphere at  $t = 70.5$  h (left panel) and  $t = 97.3$  h (right panel).

magnetosphere are shown by green, while the last closed field lines in the tail are shown by red.

During the simulated CME event  $B_z$  varies between about 0 and 3 nT, therefore the global magnetospheric configuration never switches to pure “South” or “North” configuration. However, the magnetosphere significantly changes during the event. As the solar wind dynamic pressure increases the dayside magnetopause moves inward and the current densities significantly increase. In addition, the magnetosphere becomes narrower and the length of the magnetic wings increases from about  $60R_E$  to  $90R_E$ . Overall, the energy and magnetic flux stored in the magnetosphere increased substantially.

A very interesting feature seen in Fig. 4 is the clockwise “twist” of the magnetosphere perpendicular to the solar wind direction. This twist, which is particularly visible in the wings, is due to the presence of a non-zero  $B_y$  component.

Fig. 5 shows the change of ionospheric potential and convection pattern during the CME event. The color code

represents the calculated electric potential in the height-integrated ionosphere, white lines show ionospheric convection patterns. One can see the two-cell pattern of ionospheric convection typical for southward-type IMF conditions. The convection pattern is also “twisted” due to the presence of a non-zero IMF  $B_y$  component. The most important change in the ionosphere is the doubling of the cross-cap potential drop from 30 kV at 70.5 h to 60 kV some 27 h later.

Overall, the terrestrial consequences of the simulated space weather event were not “dramatic” due to our choice of initial conditions to drive it. During the event the  $B_z$  component of the interplanetary magnetic field never exceeded +1 nT, therefore the geoeffectiveness of the CME was quite small. However, the capabilities demonstrated by doing the calculation are themselves dramatic, and nothing precludes us from using the code to simulate more geoeffective events, and ultimately even for forecasting real storms in space. This will be the focus of our upcoming investigations.

## References

- Amm, O., 1996. Comment on “A three-dimensional, iterative, mapping procedure for the implementation of an ionosphere-magnetosphere anisotropic Ohm’s law boundary condition in global magnetohydrodynamic simulations” by Michael L. Goodman. *Annales Geophysicae* 14, 773.
- Axford, W.I., McKenzie, J.F., 1996. The acceleration of the solar wind. In: Winterhalter, D., Gosling, J.T., Habbal, S.R., Kurth, W.S., Neugebauer, M. (Eds.), *Solar Wind Eight*. American Institute of Physics, Tucson, AZ, pp. 72–75.
- Axford, W.I., McKenzie, J.F., 1997. The solar wind. In: Jokipii, J.R., Sonett, C.P., Giampapa, M.S. (Eds.), *Cosmic Winds and the Heliosphere*. University of Arizona Press, Tucson, pp. 31–66.
- Berchem, J., Raeder, J., Ashour-Abdalla, M., 1995. Reconnection at the magnetospheric boundary: results from global magnetohydrodynamic simulations. In: Song, P., Sonnerup, B., Thomsen, M. (Eds.), *Physics of the Magnetopause*. AGU, Washington, DC, p. 205.
- Brecht, S., Lyon, J., Fedder, J., Hain, K., 1981. A simulation study of east–west IMF effects on the magnetosphere. *Geophysical Research Letters* 8, 397.
- Brecht, S., Lyon, J., Fedder, J., Hain, K., 1982. A time-dependent three-dimensional simulation of the earth’s magnetosphere: reconnection events. *Journal of Geophysical Research* 87, 6098.
- Dryer, M., 1998. Multidimensional, magnetohydrodynamic simulation of solar-generated disturbances: space weather forecasting of geomagnetic storms. *AIAA Journal* 3, 365–370.
- Dryer, M., Wu, S., Steinolfson, R.S., Wilson, R.M., 1979. Magnetohydrodynamic models of coronal transients in the meridional plane. II. Simulation of the coronal transient of 1973 August 21. *Solar Physics* 227, 1059.
- Fedder, J.A., Lyon, J.G., 1987. The solar wind-magnetosphere-ionosphere current-voltage. *Geophysical Research Letters* 14, 880.
- Fedder, J.A., Lyon, J.G., Slinker, S.P., Mobarri, C.M., 1995a. Topological structure of the magnetotail as a function of interplanetary magnetic field direction. *Journal of Geophysical Research* 100, 3613.
- Fedder, J.A., Slinker, S.P., Lyon, J.G., Elphinstone, R.D., 1995b. Global numerical simulation of the growth phase and the expansion onset for a substorm observed by Viking. *Journal of Geophysical Research* 100, 19,083–19,093.
- Fedder, J.A., Slinker, S.P., Lyon, J.G., 1998. A comparison of global numerical simulation results to data for the January 27–28, 1992, Geospace Environment Modeling challenge event. *Journal of Geophysical Research* 103 (A7), 14,799–14,810.
- Fisher, R.R., Poland, A.I., 1981. Coronal activity below  $2R_{\odot}$ : February 15–17. *Astrophysical Journal* 246, 1004.
- Fisk, L.A., 1996. Motion of the footpoints of heliospheric magnetic field lines at the Sun: implications for recurrent energetic particle events at high heliographic latitudes. *Journal of Geophysical Research* 101 (A7), 15,547–15,553.
- Fisk, L.A., Schwadron, N.A., Zurbuchen, T.H., 1999a. The acceleration of the fast solar wind by the emergence of new magnetic flux. *Journal of Geophysical Research* 104 (19), 765.
- Fisk, L.A., Zurbuchen, T.H., Schwadron, N.A., 1999b. On the coronal magnetic fields: consequences of large-scale motions. *Astrophysical Journal* 521, 868–877.
- Gombosi, T.I., De Zeeuw, D.L., Groth, C.P.T., Powell, K.G., Song, P., 1998. The length of the magnetotail for northward IMF: results of 3D MHD simulations. In: Chang, T., Jasperse, J.R. (Eds.), *Physics Space Plasmas* (1998), Vol. 15. MIT Press, Cambridge, pp. 121–128.
- Gombosi, T.I., De Zeeuw, D.L., Groth, C.P.T., Powell, K.G., 2000. Magnetospheric configuration for Parker-spiral IMF conditions: results of a 3D AMR MHD simulation. *Advances in Space Research*, 26 (1), 139–149.
- Gombosi, T.I., Powell, K.G., De Zeeuw, D.L., 1994. Axisymmetric modeling of cometary mass loading on an adaptively refined grid: MHD results. *Journal of Geophysical Research* 99, 21,525.
- Goodman, M.L., 1995. A three-dimensional, iterative, mapping procedure for the implementation of an ionosphere-magnetosphere anisotropic Ohm’s law boundary condition in global magnetohydrodynamic simulations. *Annales Geophysicae* 13, 843.
- Groth, C.P.T., De Zeeuw, D.L., Powell, K.G., Gombosi, T.I., Stout, Q.F., 1999. A parallel solution-adaptive scheme for ideal magnetohydrodynamics, *Proceedings of AIAA 14th Computational Fluid Dynamics Conference*, AIAA Paper No. 99-3273.
- Groth, C.P.T., De Zeeuw, D.L., Gombosi, T.I., Powell, K.G., 2000. Global 3D MHD simulation of a space weather event: CME formation, interplanetary propagation, and interaction with the magnetosphere. *Journal of Geophysical Research*, in press.
- Guo, W.P., Wu, S.T., 1998. A magnetohydrodynamic description of coronal helmet streamers containing a cavity. *Astrophysical Journal* 494, 419–429.
- Hirayama, T., 1974. Theoretical models of flares and prominences. i. evaporating flare model. *Solar Physics* 34, 323.
- Holzer, T.E., Hansteen, V.H., Leer, E., 1997. Acceleration of the solar wind. In: Jokipii, J.R., Sonett, C.P., Giampapa, M.S. (Eds.), *Cosmic Winds and the Heliosphere*. University of Arizona Press, Tucson, pp. 239–257.
- Hu, Y.Q., Esser, R., Habbal, S.R., 1997. A fast solar wind model with anisotropic proton temperature. *Journal of Geophysical Research* 102, 14,661.
- Hundhausen, A.J., 1995. Coronal mass ejections: a summary of SMM observations from 1980 and 1984–1989. In: Strong, K.,

- Soba, J., Haisch, B. (Eds.), *The Many Faces of the Sun*. Springer, New York.
- Illing, R.M.E., Hundhausen, A.J., 1986. Disruption of a coronal streamer by an eruptive prominence and coronal mass ejection. *Journal of Geophysical Research* 91, 10,951.
- Janhunen, P., 1996. GUMICS-3: a global ionosphere-magnetosphere coupling simulation with high ionospheric resolution. *Proceedings of ESA 1996 Symposium on Environment Modelling for Space-based Applications*, ESA SP-392, pp 233–239.
- Janhunen, P., Koskinen, H.E.J., 1997. The closure of Region-1 field-aligned current in MHD simulation. *Geophysical Research Letters* 24 (11), 1419–1422.
- Kageyama, A., Watanabe, K., Sato, T., 1992. A global simulation of the magnetosphere with a long tail: no interplanetary magnetic field. *Journal of Geophysical Research* 97, 3929.
- Kopp, R., Pneuman, G.W., 1976. Magnetic reconnection on the corona and the loop prominence phenomenon. *Solar Physics* 50, 85.
- LeBoeuf, J.N., Tajima, T., Kennel, C.F., Dawson, J.M., 1981. Global simulations of the three-dimensional magnetosphere. *Geophysical Research Letters* 8, 257.
- Linker, J.A. et al., 1999. Magnetohydrodynamic modeling of the solar corona during Whole Sun Month. *Journal of Geophysical Research* 104 (A5), 9809–9830.
- Linker, J.A., Mikić, Z., 1995. Disruption of a helmet streamer by photospheric shear. *Astrophysical Journal* 438, L45–L48.
- Linker, J.A., Mikić, Z., Schnack, D.D., 1994. Modeling coronal evolution. *Proceedings of the Third SOHO Workshop*, ESA, Estes Park, Colorado, pp. 249–252.
- Lionello, R., Mikić, Z., Schnack, D.D., 1998. Magnetohydrodynamics of solar coronal plasmas in cylindrical geometries. *Journal of Computational Physics* 140, 172–201.
- Low, B.C., 1977. Evolving force-free magnetic fields. I. The development of the preflare stage. *Astrophysical Journal* 212, 234.
- Low, B.C., 1981. Eruptive magnetic fields. *Astrophysical Journal* 251, 352.
- Low, B.C., 1990. Equilibrium and dynamics of coronal magnetic fields. *Annual Review of Astronomy and Astrophysics* 28, 491.
- Low, B.C., 1994. Magnetohydrodynamic processes in the solar corona: flares, coronal mass ejections, and magnetic helicity. *Plasma Physics* 1, 1684.
- Low, B.C., 1996. Solar activity and the corona. *Solar Physics* 167, 217.
- Low, B.C., Munro, R.H., Fisher, R.R., 1982. The initiation of a coronal transient. *Astrophysical Journal* 254, 335.
- Lyon, J.G., Fedder, J., Huba, J., 1986. The effect of different resistivity models on magnetotail dynamics. *Journal of Geophysical Research* 91, 8057.
- McComas, D.J. et al., 1998. Ulysses' return to the slow solar wind. *Geophysical Research Letters* 25, 1–4.
- Mikić, Z., Barnes, D., Schnack, D.D., 1988. Evolution of a solar coronal magnetic field arcade. *Astrophysical Journal* 328, 830.
- Mikić, Z., Linker, J.A., 1994. Disruption of coronal magnetic field arcades. *Astrophysical Journal* 430, 898–912.
- Moore, R.L., Falconer, D.A., Porter, J.G., Suess, S.T., 1999. Coronal heating by magnetic explosions. *Space Science Reviews* 87, 283–286.
- Neugebauer, M. et al., 1998. Spatial structure of the solar wind and comparisons with solar data and models. *Journal of Geophysical Research* 103, 14,587–14,599.
- Odrščil, D., Pizzo, V.J., 1999a. Distortion of the interplanetary magnetic field by three-dimensional propagation of coronal mass ejections in a structured solar wind. *Journal of Geophysical Research* 104, 28,225–28,239.
- Odrščil, D., Pizzo, V.J., 1999b. Three-dimensional propagation of CMEs in a structured solar wind flow, 1, CME launched within the streamer belt. *Journal of Geophysical Research* 104, 483–492.
- Odrščil, D., Pizzo, V.J., 1999c. Three-dimensional propagation of coronal mass ejections in a structured solar wind flow, 2, CME launched adjacent to the streamer belt. *Journal of Geophysical Research* 104, 493–503.
- Ogino, T., 1986. A three-dimensional MHD simulation of the interaction of the solar wind with the Earth's magnetosphere: the generation of field-aligned currents. *Journal of Geophysical Research* 91, 6791.
- Ogino, T., Walker, R.J., 1984. A magnetohydrodynamic simulation of the bifurcation of tail lobes during intervals with a northward interplanetary magnetic field. *Geophysical Research Letters* 11, 1018.
- Ogino, T., Walker, R., Ashour-Abdalla, M., 1989. A magnetohydrodynamic simulation of the formation of magnetic flux tubes at the Earth's dayside magnetopause. *Geophysical Research Letters* 16, 155.
- Ogino, T., Walker, R., Ashour-Abdalla, M., Dawson, J., 1986. An MHD simulation of the effects of the interplanetary magnetic field  $B_y$  component on the interaction of the solar wind with the Earth's magnetosphere during southward interplanetary magnetic field. *Journal of Geophysical Research* 91, 10,029.
- Parker, E.N., 1963. *Interplanetary Dynamical Processes*. Interscience, New York.
- Pizzo, V.J., 1991. The evolution of corotating stream fronts near the ecliptic plane in the inner solar system 2. Three-dimensional tilted-dipole fronts. *Journal of Geophysical Research* 96 (A4), 5405.
- Powell, K.G., 1994. An approximate Riemann solver for magnetohydrodynamics (that works in more than one dimension). *Technical Report 94-24*, ICASE, Langley, VA.
- Powell, K.G., Roe, P.L., Myong, R.S., Gombosi, T.I., DeZeeuw, D.L., 1995. An upwind scheme for magnetohydrodynamics. *Proceedings of AIAA 12th Computational Dynamics Conference*, San Diego, AIAA-95-1704, p. 661.
- Powell, K.G., Roe, P.L., Linde, T.J., Gombosi, T.I., DeZeeuw, D.L., 1999. A solution-adaptive upwind scheme for ideal magnetohydrodynamics. *Journal of Computational Physics* 154 (2), 284–309.
- Pulkkinen, T., Baker, D., Walker, R., Raeder, J., Ashour-Abdalla, M., 1995. Comparison of empirical magnetic field models and global MHD simulations: the near-tail currents. *Geophysical Research Letters* 22, 675–678.
- Pulkkinen, T.I., Baker, D.N., Wiltberger, M., Goodrich, C., Lopez, R.E., Lyon, J.G., 1998. Pseudobreakup and substorm onset: observations and MHD simulations compared. *Journal of Geophysical Research* 103 (A7), 14,847–14,854.
- Raeder, J., Berchem, J., Ashour-Abdalla, M., 1998. The geospace environment modeling grand challenge: results from a global geospace circulation model. *Journal of Geophysical Research* 103 (A7), 14,787–14,797.
- Raeder, J., Berchem, J., Ashour-Abdalla, M., Frank, L.A., Paterson, W.R., Ackerson, K.L., Kokubun, S., Yamamoto, T., Slavin, J.A., 1997. Boundary layer formation in the magnetotail: geotail

- observations and comparisons with a global MHD simulation. *Geophysical Research Letters* 24, 951–954.
- Raeder, J., Walker, R.J., Ashour-Abdalla, M., 1995. The structure of the distant geomagnetic tail during long periods of northward IMF. *Geophysical Research Letters* 22, 349.
- Schwadron, N.A., Fisk, L.A., Zurbuchen, T.H., 1999. Elemental fractionation in the slow solar wind. *Astrophysical Journal* 521, 859–867.
- Steinolfson, R.S., 1992. Three-dimensional structure of coronal mass ejections. *Journal of Geophysical Research* 97, 10,811–10,824.
- Steinolfson, R.S., 1994. Modeling coronal streamers and their eruption. *Space Science Reviews* 70, 289–294.
- Suess, S.T., Wang, A.-H., Wu, S.T., 1996. Volumetric heating in coronal streamers. *Journal of Geophysical Research* 101 (A9), 19,957–19,966.
- Tanaka, T., 1995. Generation mechanisms for magnetosphere–ionosphere current systems deduced from a three-dimensional MHD simulation of the solar wind–magnetosphere–ionosphere coupling process. *Journal of Geophysical Research* 100 (A7), 12,057–12,074.
- Usadi, A., Kageyama, A., Watanabe, K., Sato, T., 1993. A global simulation of the magnetosphere with a long tail: southward and northward interplanetary magnetic field. *Journal of Geophysical Research* 98, 7503.
- Usmanov, A.V., 1995. Numerical 3-D time-dependent MHD model of the solar wind. *Space Science Reviews* 72, 121.
- van Ballegoijen, A.A., Martens, P.C.H., 1990. Magnetic fields in quiescent prominences. *Astrophysical Journal* 361, 283.
- Walker, R.J., Ogino, T., Raeder, J., Ashour-Abdalla, M., 1993. A global magnetohydrodynamic simulation of the magnetosphere when the interplanetary magnetic field is southward: the onset of magnetotail reconnection. *Journal of Geophysical Research* 98, 17,235.
- Wang, A.-H., Wu, S.T., Suess, S.T., Poletto, G., 1998. Global model of the corona with heat and momentum addition. *Journal of Geophysical Research* 103, 1913–1922.
- Watanabe, K., Sato, T., 1990. Global simulation of the solar wind–magnetosphere interaction: the importance of its numerical validity. *Journal of Geophysical Research* 95, 75.
- White, W.W., Siscoe, G.L., Erickson, G.M., Kaymaz, Z., Maynard, N.C., Siebert, K.D., Sonnerup, B.U.Ö., Weimer, D.R., 1998. The magnetospheric sash and the cross-tail S. *Geophysical Research Letters* 25 (10), 1605–1608.
- Winglee, R.M., Papitashvili, V.O., Weimer, D.R., 1997. Comparison of the high-latitude ionospheric electrodynamics inferred from global simulations and semiempirical models for the January 1992 GEM campaign. *Journal of Geophysical Research* 102, 26,961–26,977.
- Wu, C.C., Walker, R., Dawson, J.M., 1981. A three-dimensional MHD model of the Earth's magnetosphere. *Geophysical Research Letters* 8, 523.
- Wu, S.T., Guo, W.P., 1997. A self-consistent numerical magnetohydrodynamic (MHD) model of helmet streamer and flux rope interactions: initiation and propagation of coronal mass ejections (CMEs). In: Crooker, N., Joselyn, J., Feynman, J. (Eds.), *Coronal Mass Ejections*, Vol. 99. American Geophysical Union, Washington, DC, pp. 83–89.
- Wu, S.T., Hu, Y.Q., Nakagawa, Y., Tandberg-Hanssen, E., 1983. Induced mass and wave motions in the lower solar atmosphere. I. Effects of shear motion on flux tubes. *Astrophysical Journal* 266, 866.